

Ab initio mobility of mono-layer MoS₂ and WS₂: comparison to experiments and impact on the device characteristics

Y. Lee, S. Fiore, and M. Luisier

Integrated Systems Laboratory, ETH Zurich, Zurich, Switzerland, email: youslee@iis.ee.ethz.ch

Abstract—We combine the linearized Boltzmann Transport Equation (LBTE) and quantum transport by means of the Non-equilibrium Green's Functions (NEGF) to simulate single-layer MoS₂ and WS₂ ultra-scaled transistors with carrier mobilities extracted from experiments. Electron-phonon, charged impurity, and surface optical phonon scattering are taken into account with all necessary parameters derived from *ab initio* calculations or measurements, except for the impurity concentration. The LBTE method is used to scale the scattering self-energies of NEGF, which only include local interactions. This ensures an accurate reproduction of the measured mobilities by NEGF. We then perform device simulations and demonstrate that the considered transistors operate far from their performance limit (from 50% for MoS₂ to 60% for WS₂). Higher quality materials and substrate engineering will be needed to improve the situation.

I. Introduction

Motivated by the first demonstration of a mono-layer MoS₂ transistor [1] significant efforts have been undertaken to simulate the properties of devices based on 2-D transition metal dichalcogenides (TMDs). Their carrier mobility has been extensively modeled, starting with Ref. [2]: the phonon-limited mobility of MoS₂ was computed with the linearized Boltzmann Transport Equation (LBTE) after extracting the required effective masses and electron-phonon coupling parameters from density-functional theory (DFT). Going one step further, the influence of charged impurity scattering was highlighted in Ref. [3], that of surface optical phonons in Ref. [4], in both cases in the effective mass approximation.

Accurately predicting the “current vs. voltage” characteristics of monolayer TMD transistors represents another challenge. It can be addressed with an *ab initio* quantum transport (QT) approach, e.g. the Non-equilibrium Green's Functions (NEGF), expressed in a maximally localized Wannier function (MLWF) basis. As such calculations are computationally very demanding, they were first restricted to ballistic transport [5]. Electron-phonon scattering was later added, but in the form of parameterized self-energies [6]. Attempts were also made to treat the electrons, phonons, and their interactions at the *ab initio* level [7]. However, because of the diagonal approximation typically applied to the scattering self-energies, the obtained results may suffer from inaccuracies.

Here, we combine LBTE and NEGF, both from first-principles, to provide the first QT simulations of MoS₂ and WS₂ single-layer transistors with the same mobility values as in experiments. By considering electron-phonon (E-Ph), charged impurity (CI), and surface optical phonon (SOP) scattering, LBTE can reproduce the experimental mobility of these 2-D

materials over a large temperature range. These results were then used to scale each diagonal scattering self-energy in NEGF so that our QT calculations produce the same mobilities as LBTE. The simulated “I-V” characteristics finally suggest that CI and SOP, whose magnitude can be altered by improving the 2-D crystal quality or by changing the substrate material, are responsible for a current reduction by a factor comprised between 1.7 (WS₂) and 2 (MoS₂), as compared to the case with E-Ph only (performance limit).

II. Approach

Our *ab initio* LBTE+QT approach is summarized in Fig. 1. As first step, the electronic structures of the primitive unit cell corresponding to a 2-D monolayer were computed with VASP [8] within the generalized gradient approximation (GGA) of Perdew, Burke, and Ernzerhof (PBE) [9]. For transport calculations, the resulting plane-wave DFT results were projected onto a MLWF basis [10] to produce a tight-binding-like Hamiltonian [11]. The dynamical matrices required for the phonon frequencies were generated via density-functional perturbation theory (DFPT) and the Phonopy code [12].

For each interaction type (E-Ph, CI, and SOP), a specific scattering self-energy $\Sigma(E, k)$ (NEGF) and transition probability function $S(b, \mathbf{k}|b', \mathbf{k}')$ (LBTE) was constructed from the prepared DFT data and the corresponding Feynman diagram. In case of E-Ph, the equations of Refs. [11] and [13] were implemented for NEGF and LBTE, respectively. The electron-SOP coupling was modeled by taking into account the vibrations of the dielectric environments surrounding the 2-D monolayers [4]. The phonon frequencies and coupling strengths were taken from measurements [14]. Finally, the electron-CI interactions were cast into a Coulomb potential with image charges [3] using the impurity concentration n_{imp} as fitting parameter. 2-D screening caused by the surrounding dielectrics was applied to damp SOP and CI scattering.

For each 2-D material, three mobilities μ_{E-Ph} , μ_{SOP} , and μ_{CI} were calculated with the modified LBTE solver of Ref. [13], accounting for local and non-local energy-momentum transitions. Available temperature-dependent experimental data were then reproduced by adjusting n_{imp} only. Next, the same mobilities were computed with NEGF using the “dR/dL” method [15] and assuming diagonal scattering self-energies. By comparing the values obtained with LBTE and NEGF, renormalization factors (λ_{E-Ph} , λ_{SOP} , and λ_{CI}) could be determined to scale $\Sigma_{E-Ph}(E, k)$, $\Sigma_{SOP}(E, k)$, and $\Sigma_{CI}(E, k)$, ensuring that NEGF returns the same mobility as LBTE and experiments.

Taking advantage of the “calibrated” NEGF simulator [11], the I-V characteristics of 2-D devices could be accurately predicted.

III. Results

The low-field mobility of MoS₂ and WS₂ monolayers as a function of temperature is reported in Fig. 2. Three cases were investigated: MoS₂ deposited on a 270 nm-thick bottom SiO₂ substrate (i) with and (ii) without a 30 nm-thick top HfO₂ layer and (iii) WS₂ with the same substrate as (ii). For the MoS₂ configuration (i), the temperature-dependence of the E-Ph-, SOP-, and CI-limited mobilities, as obtained with LBTE, is plotted in Fig. 2(a), together with the total mobility calculated by Matthiessen’s rule. The impurity concentration was set to $n_{imp}=2.5e12\text{ cm}^{-2}$, which leads to an excellent agreement with the experimental data of Ref. [16] (Fig. 2(b)). It can be seen that CI scattering is the limiting factor at all temperatures, but SOP kicks in at high temperatures and induces a significant mobility drop. The LBTE mobilities of the second MoS₂ sample (Fig. 2(c), $n_{imp}=1.5e12\text{ cm}^{-2}$) [17] and of WS₂ (Fig. 2(d), $n_{imp}=1.35e12\text{ cm}^{-2}$) [18] reveal an equally good agreement with experiments. In Fig. 2 we also provide the room-temperature QT mobilities with renormalized scattering self-energies to validate our scheme.

As next step, the “current vs. voltage” characteristics of MoS₂ and WS₂ monolayer field-effect transistors (FETs) are analyzed. The selected benchmark structure is shown in Fig. 3(a): a single-gate (SG) FET with a gate length $L_g=15$ or 50 nm, source/drain-extensions of $L_s=L_d=15$ nm each, and a supply voltage $V_{DD}=0.7$ V. The 2-D materials were deposited on a SiO₂ “substrate” with a top HfO₂ layer of thickness $t_{ox}=3$ nm and a relative permittivity $\epsilon_{ox}=20$. Ohmic contacts were assumed with a donor concentration $N_D=5e13\text{ cm}^{-2}$. Hence, the effect of contact resistances was neglected. To verify that the QT scattering models properly work, the energy- and position-resolved current of the WS₂ FET is depicted in Fig. 3(b), including E-Ph, SOP, and CI interactions, while current conservation is demonstrated in Fig. 3(c) for different gate biases. As expected, electrons lose a substantial amount of their energy on the drain side of the transistor, where the electric field reaches its maximum.

The I_d-V_{gs} transfer characteristics of both FET types are shown in Figs. 4(a-b). Two curves per device were computed. First, as a reference, the current with electron-phonon scattering only is given. This mechanism cannot be eliminated, contrary to CI that can be reduced by improving the crystal quality or SOP that could possibly be minimized by carefully choosing the substrate material. The second curve includes all scattering sources and uses the impurity concentrations and scaling factors from Fig. 2. A strong ON-current decrease caused by SOP and CI is found. It is larger in MoS₂ than in WS₂ (2 vs. 1.7 \times) due to the presence of more charged impurities ($n_{imp}=2.5$ vs. 1.35 cm^{-2}). Consequently, both FETs operate far from their optimum, defined as the current with E-Ph scattering only. It can be noticed in Fig. 4(c) that the gate capacitance $C_g=5.8\text{ }\mu\text{F}/\text{cm}^2$ extracted from the derivative of the electron concentration at the top-of-the-barrier with respect to the gate voltage does not suffer

from so-called density-of-states bottlenecks as it approaches the value of $C_{ox}=\epsilon_{ox}/t_{ox}=5.9\text{ }\mu\text{F}/\text{cm}^2$, the oxide capacitance.

The influence of SOP and CI is examined in Fig. 5(a) where the ON-current values of the MoS₂ and WS₂ FETs are plotted as a function of the impurity concentration n_{imp} . The cases with E-Ph scattering only, E-Ph+SOP, and E-Ph+SOP+CI are supplied, thus isolating the impact of each scattering mechanism from the others. It appears that SOP contributes slightly more to the current decrease than CI (factor 1.37-1.5 \times vs. 1.3-1.34 \times), for both 2-D materials, contrary to what was observed in mobility calculations (CI-limited). This seems to indicate that the emission/absorption of SOP is enhanced under high-field conditions. The corresponding injection velocities at the top-of-the-barrier follow in Fig. 5(b). Thanks to their lower effective mass ($m_e^*=0.30$ vs. 0.46 m_0), electrons in WS₂ are faster than in MoS₂, but their velocity could still be improved by a factor ~ 2 , as compared to the present case, if both SOP and CI were removed. The extracted velocities however degrade when the gate length increases to 50 nm, as can be seen in Table 5(c). The latter summarizes the key mobility, ON-current, and injection velocity results obtained here.

IV. Conclusion

We proposed an *ab initio* LBTE+QT framework to compute the transport properties of 2-D materials. It relies on the renormalization of the NEGF self-energies with scaling factors determined from LBTE. The mobility of MoS₂ and WS₂ monolayers was accurately modeled with this method, which also helped predict the “I-V” characteristics of monolayer MoS₂ and WS₂ FETs with short gate lengths. Further device progresses will depend on improved materials and careful design choices. The developed environment is now ready to explore novel 2-D compounds beyond TMDs.

Acknowledgment

This work was supported the MARVEL National Centre of Competence in Research of the Swiss National Science Foundation (SNSF), by SNSF under Grant No. 175479 (ABIME), and by a grant from the Swiss National Supercomputing Centre (CSCS) under Project s876.

References

- [1] B. Radisavljevic et al., Nat. Nano. 6, 147 (2011).
- [2] K. Kaasbjerg et al., Phys. Rev. B 85, 115317 (2012).
- [3] Z.-Y. Ong et al., Phys. Rev. B 88, 165316 (2013).
- [4] N. Ma and D. Jena, Phys. Rev. X 4, 011043 (2014).
- [5] J. Chang et al., App. Phys. Lett. 103, 223509 (2013).
- [6] A. Sengupta et al., AIP Advances 5, 027101 (2015).
- [7] M. Luisier et al., Proc. of IEDM 2016, 5.4.1-5.4.4 (2016).
- [8] G. Kresse and J. Furthmüller, Phys. Rev. B 54, 11169 (1996).
- [9] J. P. Perdew et al., Phys. Rev. Lett. 77, 3865 (1997).
- [10] A. A. Mostofi et al., Comp. Phys. Comm. 178, 685-699 (2008).
- [11] A. Szabó et al., Phys. Rev. B 92, 035435 (2015).
- [12] A. Togo et al., Phys. Rev. B 78, 134106 (2008).
- [13] R. Rhyner and M. Luisier, J. Appl. Phys. 114, 223708 (2013).
- [14] K. Zou et al., Phys. Rev. Lett. 105, 126601 (2010).
- [15] K. Rim et al., Proc. of IEDM 2002, 43-46 (2002).
- [16] B. Radisavljevic and A. Kis, Nat. Mat. 12, 815 (2013).
- [17] K. K. H. Smithe et al., Nano. Lett. 18, 4516 (2018).
- [18] D. Ovchinnikov et al., ACS Nano 8, 8174-8181 (2014).

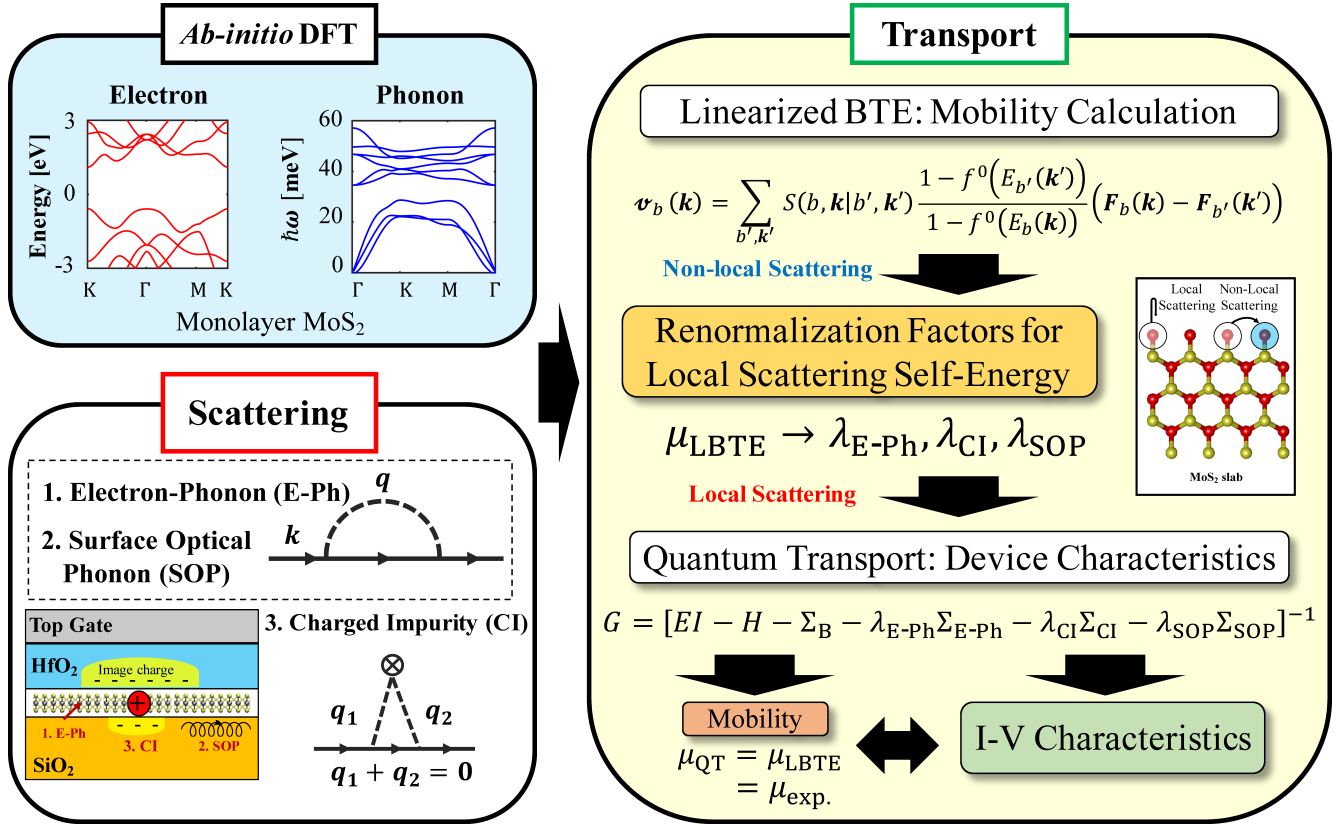


Fig. 1. Flowchart of the *ab initio* simulation framework combining LBTE and quantum transport with NEGF. First, DFT is used to construct the Hamiltonian (electron) and dynamical (phonon) matrices of monolayer MoS₂ and WS₂ transistor structures. NEGF scattering self-energies ($\Sigma(E, k)$) and LBTE transition probability functions ($S(b, k|b', k')$) are then prepared for each interaction type (E-Ph, SOP, and CI) based on the corresponding Feynman diagrams. Screening is taken into account for SOP and CI. Mobility values are first computed with *ab initio* LBTE, adjusting only the charged impurity concentration in order to reproduce experimental data over temperature. By comparing each mobility contribution (μ_{E-Ph} , μ_{SOP} , and μ_{CI}) obtained with LBTE to its NEGF counterpart, renormalization factors λ_{E-Ph} , λ_{SOP} , and λ_{CI} can be determined for each local scattering self-energy. After scaling the Σ 's with the λ 's, the NEGF quantum transport solver produces the same mobilities as LBTE and can therefore accurately predict device characteristics.

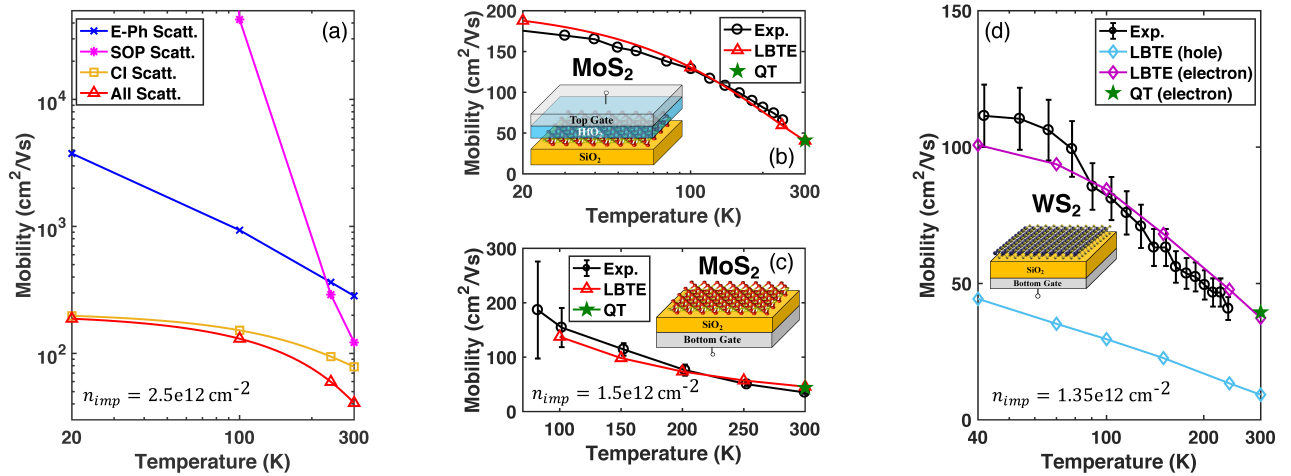


Fig. 2. (a) Temperature-dependent electron mobility contributions as calculated by LBTE. The E-Ph- (μ_{E-Ph} , blue line with crosses), SOP- (μ_{SOP} , pink line with asterisks), and CI-limited (μ_{CI} , yellow line with squares) values are shown, together with the total mobility (red line with triangles) resulting from Matthiessen's rule. A monolayer MoS₂ with a 30 nm-thick top HfO₂ ($\epsilon_{ox}=20$) layer and a 270 nm-thick bottom SiO₂ ($\epsilon_R=3.9$) substrate was used for that purpose. (b) Comparison of the temperature-dependent electron mobility calculated by LBTE (red line with triangles) to experimental data (black line with circles) [16] for the same MoS₂ device as in (a) with $n_{imp}=2.5e12 \text{ cm}^{-2}$. The green star refers to the NEGF mobility after scaling the scattering self-energies. (c) Same as (b), but for a MoS₂ monolayer deposited on a 270 nm-thick SiO₂ substrate with $n_{imp}=1.5e12 \text{ cm}^{-2}$ [17]. (d) Same as (b) and (c), but for a WS₂ monolayer on a 270 nm-thick SiO₂ substrate with $n_{imp}=1.35e12 \text{ cm}^{-2}$ [18] (black line with circles: experiment, lines with diamonds: LBTE).

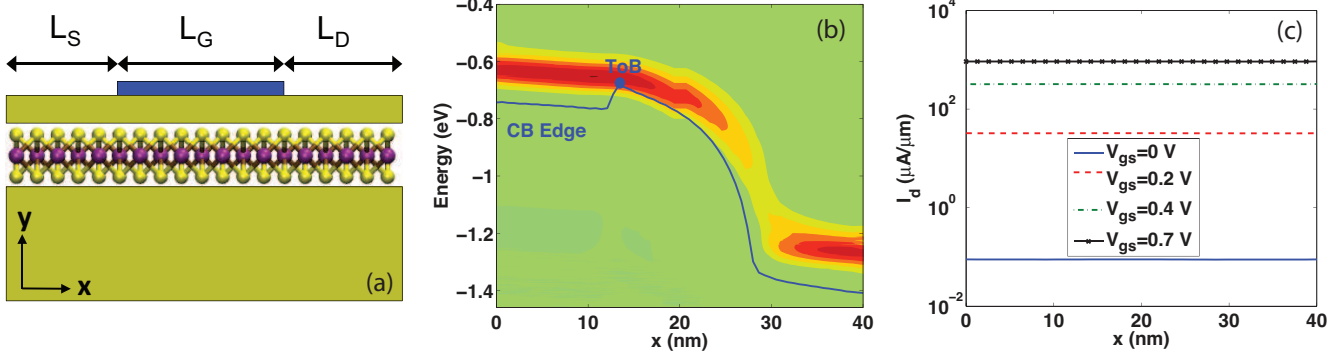


Fig. 3. (a) Schematic view of the single-gate (SG) monolayer MoS₂ and WS₂ field-effect transistors (FETs) investigated here. The source and drain extensions measure $L_s=L_d=15$ nm each and are doped with a donor concentration $N_D=5e13$ cm⁻². Ohmic contacts are assumed. The gate length L_g is set to 15 or 50 nm. The 2-D materials lie on a 20 nm thick SiO₂ “substrate” with $\epsilon_R=3.9$. The gate contact is separated from the channel by a $t_{ox}=3$ nm HfO₂ layer with $\epsilon_{ox}=20$. All device simulations were performed at $V_{ds}=0.7$ V and at room temperature. (b) Spectral distribution of the current through the WS₂ FET with $L_g=15$ nm, $V_{gs}=V_{ds}=0.7$ V, and in the presence of all scattering mechanisms considered in this work. Red indicates high current concentrations, green none. The blue line refers to the conduction band edge of WS₂. (c) Spatial current distribution of the same WS₂ device as in (b) as a function of V_{gs} and the position along the x transport direction. All scattering sources discussed in this paper are included.

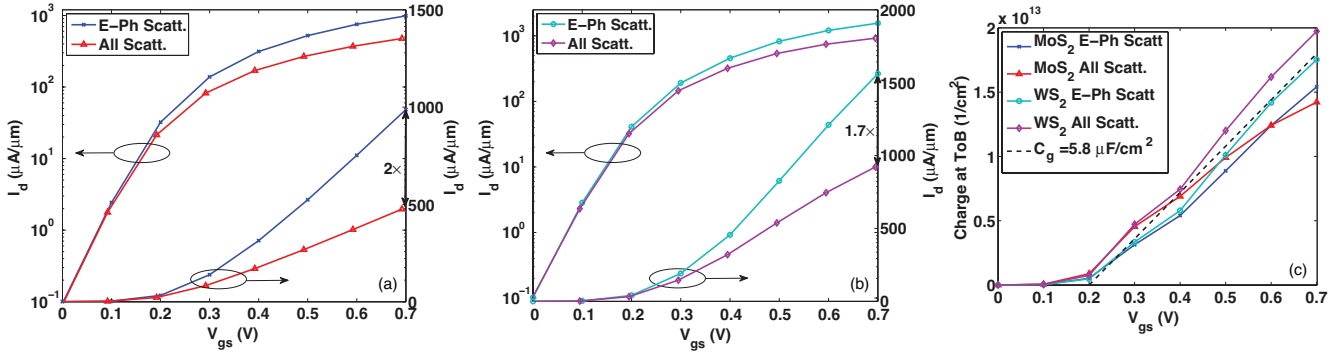


Fig. 4. (a) I_d - V_{gs} transfer characteristics of the monolayer MoS₂ single-gate FET plotted on a linear (right y -axis) and on a logarithmic (left y -axis) scale. The current with electron-phonon scattering only (blue lines with crosses) and with all scattering sources (red lines with triangles) are reported at $V_{ds}=0.7$ V, $I_{OFF}=0.1$ $\mu A/\mu m$, and with a charged impurity concentration $n_{imp}=2.5e12$ cm⁻². (b) Same as (a), but for the WS₂ FET and $n_{imp}=1.35e12$ cm⁻². (c) Electron concentration extracted at the top-of-the-barrier (ToB, see Fig. 3) as a function of V_{gs} for the four cases presented in (b) and (c). An average gate capacitance $C_g=5.8$ $\mu F/cm^2$ can be extracted from these results (dashed black line), closed to the oxide capacitance $C_{ox}=t_{ox}/\epsilon_{ox}=5.9$ $\mu F/cm^2$.

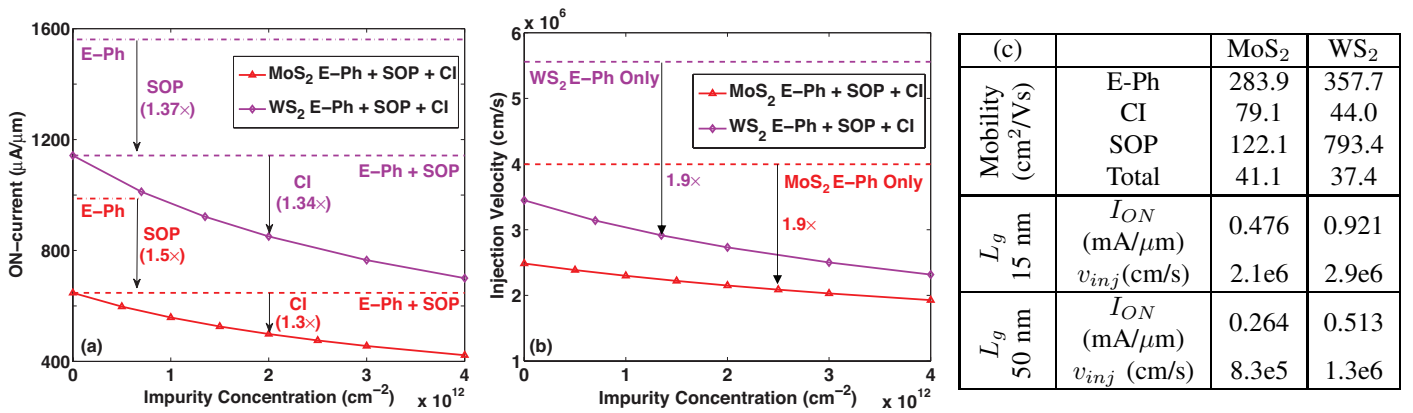


Fig. 5. (a) ON-current at $I_{OFF}=0.1$ $\mu A/\mu m$ as a function of the charged impurity concentration for the MoS₂ (red line with triangle) and WS₂ (purple line with diamonds) single-gate FET. E-Ph and SOP scattering are included as well. The dashed lines refer to the E-Ph+SOP (no CI) case, the dashed-dotted lines to E-Ph only. The current reductions caused by SOP and CI (at $n_{imp}=2e12$ cm⁻²) are indicated by the arrows. (b) Electron injection velocity at the ToB location corresponding to the ON-currents in (a). (c) Table summarizing the calculated room temperature mobility values (E-Ph, CI, SOP, and total) at an electron concentration $1e13$ cm⁻² ($4.8e12$ cm⁻²) for MoS₂ (WS₂) and I - V characteristics of the corresponding FETs with $n_{imp}=2.5e12$ cm⁻² ($1.35e12$ cm⁻²). The ON-current and injection velocity at the ToB are provided for devices with two different gate lengths ($L_g=15$ and 50 nm).